PCCP

COMMUNICATION

View Article Online
View Journal | View Issue

Cite this: *Phys. Chem. Chem. Phys.*, 2025, **27**, 16733

Received 23rd April 2025,
Accepted 21st July 2025

DOI: 10.1039/d5cp01547b

rsc.li/pccp

Intrinsic visible emission of amyloid-β oligomers: a potential tool for early alzheimer's diagnosis†

Mercedes Novo, *[a] Sara Illodo, [ab] Jesús Seijas, [ab] Stella Hernández, [a] Flor Rodríguez-Prieto [b] and Wajih Al-Soufi [a]

Alzheimer's disease (AD) is a major public health challenge, with its onset occurring years before symptoms appear. Soluble amyloid-β (Aβ) oligomers are key species in AD pathogenesis and diagnosis, highlighting the need for early detection. This study investigates the intrinsic fluorescence of Aβ(1–40) (Aβ40) as a label-free approach to detecting early-stage oligomers. Aβ40 exhibits autofluorescence dominated by tyrosine emission, which undergoes a strong blue shift and quenching during oligomerization. Additionally, aggregation-induced emission (AIE) in the visible spectral region emerges, correlating with Aβ oligomer concentration and providing a means to detect and quantify oligomers. At the critical aggregation concentrations cac_1 = 0.5 μM and cac_2 = 19 μM, distinct aggregation behaviours are observed. By employing steady-state fluorescence spectroscopy, a widely accessible technique, these findings establish a direct link between early Aβ aggregation and intrinsic fluorescence changes. This approach eliminates the need for extrinsic probes, simplifying experimental procedures and reducing artefacts. Although further studies are required to develop a robust quantitative correlation for potential diagnostic applications, Aβ autofluorescence represents a promising strategy for investigating early aggregation processes in the context of AD.

Alzheimer's disease (AD) constitutes one of the most significant public health challenges in ageing societies.[1] It is well-established that the onset of AD occurs several years before the first symptoms manifest, highlighting the critical need for developing methods that enable early diagnosis.[2] The formation of neurotoxic oligomers during the initial stages of amyloid-β (Aβ) aggregation is believed to be a key process in the progression of AD.[3–7] Therefore, the early detection of Aβ oligomers (AβOs) in biological fluids could represent a valuable diagnostic strategy.[8,9]

Due to the complex Aβ aggregation process, the characterization of AβOs requires specialised experimental techniques and detailed data analysis. Fluorescence correlation spectroscopy (FCS), a single-molecule technique, is a valuable tool for determining the critical aggregation concentration (cac) of Aβ and characterising its aggregates *in vitro*.[10,11] While FCS could, in principle, be applied to biological fluids, its complexity and specialised requirements limit its practicality for routine diagnostics. More conventional techniques, such as steady-state fluorescence spectroscopy, offer a broadly accessible alternative for clinical analysis.

Traditional probes such as Thioflavin T (ThT) primarily bind to amyloid fibrils rather than oligomers and are not specific to fibrillar structures.[12–14] In the past decade, new probes capable of specifically detecting oligomers have been developed.[14] These probes typically follow two main strategies: modifying the peptide backbone—through the fusion of fluorescent proteins or the attachment of chemical tags—or designing molecular probes that selectively interact with AβOs.[14] Typically, probes with strong fluorescence enhancement upon binding and high affinity to soluble AβOs are employed,[15,16] and in some cases, they enable ratiometric tracking.[17] Their suitability for *in vivo* studies[15,17] and potential for quantifying AβO in biological fluids are also significant advantages.[17,18] However, most extrinsic probes lack specificity for early soluble Aβ oligomers, as they can also bind to peptides in non-β-sheet conformations.

These limitations could potentially be addressed by exploiting the intrinsic fluorescence of the peptides, specifically their aromatic residues. The most relevant Aβ peptides, Aβ40 and Aβ42 comprising 40 and 42 amino acids, respectively contain the aromatic amino acids tyrosine and phenylalanine, with one tyrosine and three phenylalanine residues. Since tyrosine is significantly more emissive than phenylalanine, its fluorescence is expected to dominate the photophysical behaviour of these peptides.

In this work, we explore the potential of detecting AβOs through their autofluorescence by analysing their steady-state

[a] *Departamento de Química Física, Facultade de Ciencias, Campus Terra, Universidade de Santiago de Compostela, 27002 Lugo, Spain. E-mail: m.novo@usc.es*

[b] *Centro Singular de Investigación en Química Biolóxica e Materiais Moleculares (CiQUS), Facultade de Química, Departamento de Química Física, Universidade de Santiago de Compostela, 15782 Santiago de Compostela, Spain*

† Electronic supplementary information (ESI) available: Materials and methods, along with additional data, are provided. See DOI: https://doi.org/10.1039/d5cp01547b

excitation and emission spectra. The photodissociation of tyrosine in an aqueous environment, leading to the deprotonation of its phenol group, may provide a means to distinguish monomers from oligomers, as this process is likely significantly reduced in the latter.[19] Additionally, changes with incubation time in the relative contributions of the different tyrosine fluorescence lifetimes have been reported, offering a potential strategy to monitor the kinetics of the aggregation process.[20]

We investigated the autofluorescence of Aβ40 within the concentration range where its oligomerization behaviour is well-characterised from our previous work using FCS.[11] Specifically, we prepared samples under the same conditions as in our prior studies, where Aβ40 was shown to aggregate in two distinct steps, with critical aggregation concentrations of cac_1 = 0.5 μM and cac_2 = 19 μM. At the first step, which is reversible, only about 10% of Aβ molecules aggregate, primarily consisting of stable oligomers of approximately 60 Aβ units, alongside a

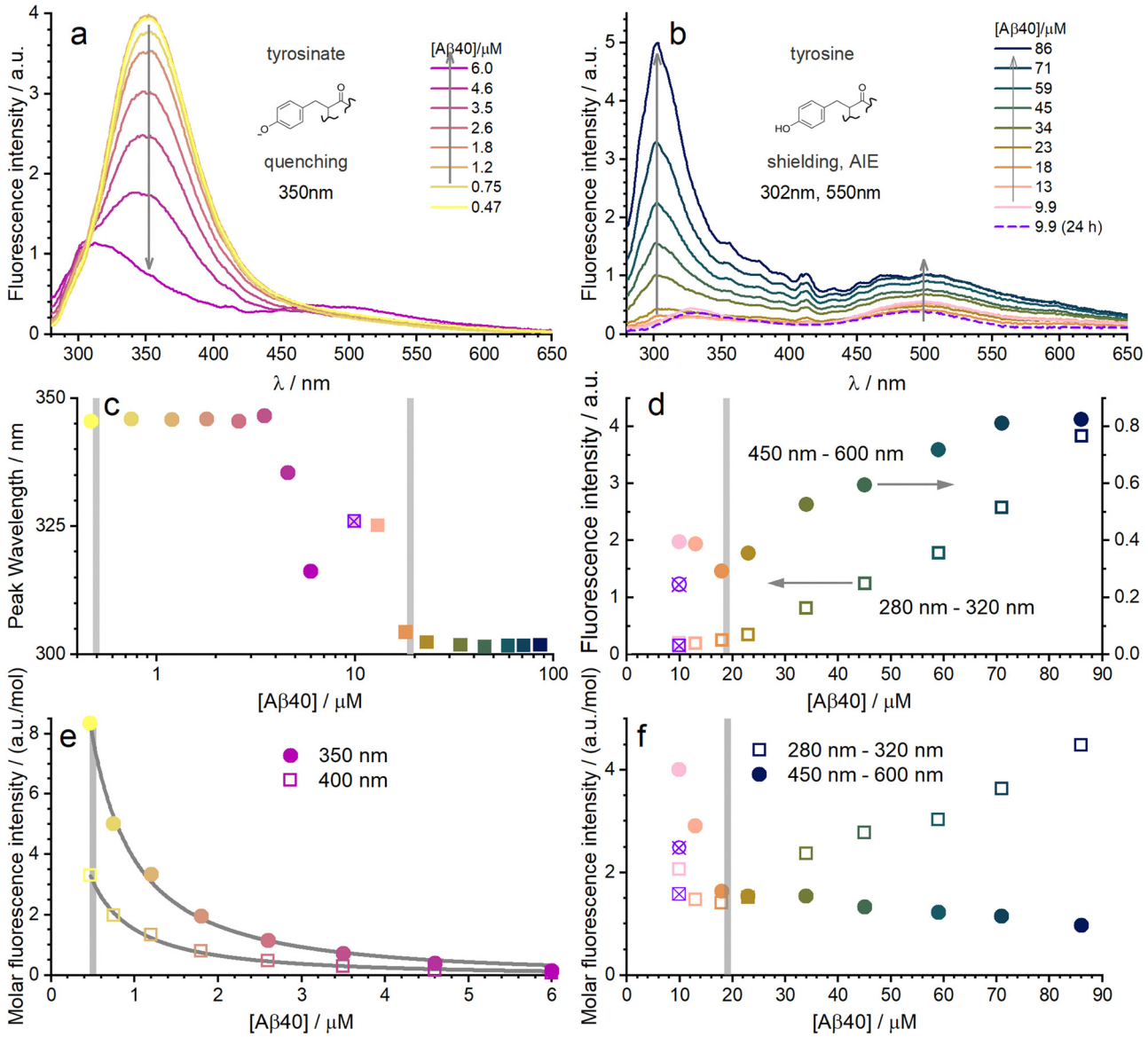

Fig. 1 (a) and (b) Corrected emission spectra of Aβ solutions in PBS with an excitation wavelength (λ_{exc}) of 245 nm: (a) low-concentration series and (b) high-concentration dilution series. Samples were prepared by serial dilution-extraction from stock solutions of 6.0 μM (a) and 86 μM (b) (see ESI†). Different cuvettes were used for each series, making the fluorescence intensities not directly comparable. Arrows indicate the direction of increasing concentration. (c) Emission maximum wavelength determined from fits of a Gaussian to the peak as a function of Aβ40 concentration. (d) Mean Fluorescence intensity in the intervals from 280 nm to 320 nm and from 450 nm to 600 nm as a function of Aβ40 concentration. (e) and (f) Molar fluorescence intensities at the indicated emission wavelengths for (e) the low-concentration series and (f) the high-concentration series. The curves in (e) represent fits using a model that combines dynamic and static quenching. Grey vertical lines indicate the critical aggregation concentrations for Aβ40, with cac_1 = 0.5 μM and cac_2 = 19 μM.[11] The violet dashed line and crossed symbols denote measurements of the most diluted sample repeated after 24 hours.

smaller population of metastable aggregates. In the second aggregation phase, the proportion of aggregated Aβ increases to around 50%, forming larger, kinetically trapped aggregates with limited reversibility. By studying Aβ40 autofluorescence across this concentration range, we aimed to correlate its intrinsic fluorescence properties with these aggregation states.

Fig. 1 presents the fluorescence emission spectra of Aβ40 obtained with excitation at 245 nm, the wavelength where the largest spectral changes were observed without distortions from the Raman band. These spectra were corrected by subtracting the weak emission of the quartz microcuvettes (Fig. S1, ESI†) from the experimental spectra (Fig. S2, ESI†). The figure presents two dilution series: (a) low-concentration and (b) high-concentration.

The spectrum at the lowest Aβ concentration in Fig. 1a), corresponding to the first cac (0.5 μM), shows an emission maximum near 350 nm, characteristic of tyrosinate – the form of tyrosine deprotonated at the phenol, formed in the excited state.[21,22] This suggests that Aβ40 is in a monomeric state where tyrosine remains exposed to the aqueous environment, allowing photodissociation of the proton. As the concentration increases within the low-concentration range (Fig. 1a), fluorescence intensity decreases strongly, initially without spectral shift, followed by a blue shift of the emission band (Fig. 1c).

If we analyse the spectral changes in the high-concentration range (Fig. 1b), the shift of the tyrosine emission band from 350 nm to 302 nm remains evident up to cac_2 (19 μM) (Fig. 1c). This blue shift of the emission band observed across the concentration range correlates with amyloid aggregation and reflects the transition from monomers to aggregates, where tyrosine molecules are shielded from the aqueous environment and no longer undergo photodissociation.[19] However, at concentrations exceeding cac_2 the position of the emission band stabilizes, indicating that the monomers are no longer contributing to the observed fluorescence.

The excitation spectra measured at 330 nm (Fig. S3a, ESI†) support this interpretation, showing a maximum around 275 nm characteristic of tyrosine absorption. A similar pattern is observed in the emission spectra with excitation at 290 nm (Fig. S4, ESI†), although with some distortions from the Raman band.

In addition to the blue shift of the tyrosine band, an anomalous emission band appears in the visible spectral region around 500 nm (Fig. 1b), where peptides typically do not emit. This blue-green fluorescence, first detectable at the highest concentration in the low-concentration series (Fig. 1a), increases in intensity as Aβ40 concentration rises (Fig. 1d), and is also observed in emission spectra recorded with excitation at 290 nm (Fig. S4c, ESI†), where the cuvette emission is minimal, ruling out experimental artefacts. The excitation spectrum for this emission (Fig. S3b, ESI†) reveals an absorption feature near 300 nm, suggesting an alternative electronic state of tyrosine in the distinct environment of aggregated peptides.

We attribute this visible emission to an aggregation-induced emission (AIE), identifying it as a characteristic feature of Aβ aggregates. Similar intrinsic fluorescence in the visible region has been previously reported for Aβ40 and Aβ42 fibres in suspension and in the solid state, where it has been linked to β-sheet-rich structures formed upon aggregation.[23–28] The appearance of this emission in soluble Aβ oligomers suggests a related phenomenon, reinforcing the idea that aggregation-induced fluorescence arises from structural rearrangements rather than from conventional aromatic fluorescence. However, the underlying mechanism remains unclear. Proposed explanations include proton transfer processes in hydrogen-bond-rich protein structures[24] or UV-light-induced oxidation of amino acids,[25] though their relevance to soluble Aβ oligomers requires further investigation.

To the best of our knowledge, this is the first reported observation of AIE in soluble Aβ oligomers. The detection of this intrinsic visible fluorescence in these early-stage aggregates suggest that it may serve as a new optical signature of amyloid aggregation. This finding opens new avenues for label-free detection and characterisation of Aβ oligomers, potentially aiding in the study of amyloid formation and its pathological implications.

The results also provide insight into the reversibility of Aβ40 aggregation, as the samples were prepared using a dilution-extraction method that assumes oligomer disaggregation upon dilution. This assumption is supported by previous FCS studies, which demonstrated that early Aβ40 oligomers are reversible upon dilution, though a kinetic barrier may delay complete disaggregation.[11]

Focusing on the low-concentration series (Fig. 1a), we observe that the characteristic visible emission associated with oligomers in the initial 6.0 μM stock solution disappears upon dilution, while the UV band shifts to longer wavelengths, indicative of monomer emission. This suggests that within this concentration range, oligomers dissociate fully upon dilution, consistent with the reported reversibility of early aggregates.[11]

In contrast, the high-concentration series exhibits partial irreversibility, as reflected in the spectra of the more diluted samples (Fig. 1b) and their intensity values (Fig. 1d), which do not follow the expected decrease in intensity. However, after 24 hours, the emission spectrum and intensity of the most dilute sample more closely resemble the expected values for this concentration, suggesting that disaggregation is not immediate but occurs gradually. This delayed equilibration is consistent with the presence of a kinetic barrier for larger aggregates, as observed in FCS studies, where oligomers formed at cac_1 (0.5 μM) were fully reversible, while larger aggregates beyond cac_2 (19 μM) exhibited limited reversibility due to kinetic constraints.[11]

To better analyse the behaviour of the emission bands as a function of concentration, the experimental fluorescence spectra (Fig. 1a and b) were normalised by dividing by the total Aβ concentration. This normalisation removes the trivial linear relationship between intensity and concentration, allowing us to examine deviations that arise from aggregation effects. The resulting spectra, now expressed as molar fluorescence intensity, are shown in Fig. S5 (ESI†). Fig. 1e and f present the

variation of these molar fluorescence intensities with the Aβ40 concentration at selected wavelengths from both emission bands. In the low-concentration range, focusing on the shorter wavelength band (Fig. 1e), the fluorescence intensity decrease is far more pronounced once the opposing concentration effect is accounted for (compare Fig. 1a *vs.* Fig. S5a, ESI†). The dramatic decrease in intensity of the 350 nm band, initially without a spectral shift (Fig. 1c), suggests collisional quenching of the tyrosinate fluorescence in monomeric Aβ. At higher Aβ concentrations (Fig. 1b and Fig. S5b, ESI†), the observed blue shift of this band, along with the emergence of the tyrosine emission band around 302 nm, indicates the formation of stable aggregates in which photodissociation of the phenolic proton is inhibited. Instrumental limitations prevented us from obtaining reliable fluorescence lifetime measurements needed to distinguish between static and dynamic quenching.

These results also indicate that tyrosinate emission in monomeric Aβ40 has a significantly higher fluorescence quantum yield than tyrosine emission in aggregates. However, strong quenching of the tyrosinate fluorescence, likely by the peptides themselves, minimizes its contribution to the observed fluorescence at concentrations around the cac_2 (Fig. 1c) where only 10% of the Aβ is aggregated.

The aggregation-induced emission band around 500 nm (Fig. S5c, ESI†) exhibits a sharp molar intensity decrease at concentrations below cac_2 (Fig. 1f and Fig. S5c, S6, ESI†), followed by a more gradual decline at higher concentrations. These changes suggest that the AIE band is sensitive to the type and size of aggregates formed. This aligns with the formation of larger aggregates beyond cac_2, which may differ structurally from oligomers. However, these data are influenced by incomplete aggregation reversibility, which may affect the applied normalization. Conversely, the increase in the tyrosine band at concentrations above cac_2, could be exploited for a ratiometric quantification method for oligomers.

The autofluorescence of Aβ40 enables tracking of the oligomerisation process through tyrosine-linked emission, which exhibits a blue shift and fluorescence quenching upon aggregation, and visible aggregation-induced emission. While these initial results demonstrate the potential of intrinsic autofluorescence for detecting early-stage Aβ oligomers, the approach remains qualitative. More detailed and extensive experiments are needed to establish a robust quantitative correlation between the autofluorescence signals and the formation of different soluble Aβ oligomers. Such studies will be essential for advancing the method towards reliable applications in early AD diagnostics.

Author contributions

Mercedes Novo: conceptualization, writing – review & editing, methodology, funding acquisition, project administration, resources, supervision. Sara Illodo: investigation, visualization. Jesús Seijas: investigation, visualization. Stella Hernández: investigation, data curation. Flor Rodríguez-Prieto: writing – review & editing, supervision. Wajih Al-Soufi: writing – review & editing, methodology, formal analysis, conceptualization, software, visualization.

Conflicts of interest

The authors declare no conflict of interests.

Data availability

The corrected emission spectra of Aβ solutions in PBS with an excitation wavelength of 245 nm of Fig. 1 are available at Zenodo at **https://doi.org/10.5281/zenodo.15199313**.

Acknowledgements

We thank the Spanish Ministerio de Ciencia e Innovación for their financial support (PID2020-120378RB-I00). S. I. and S. H. thank the Xunta de Galicia for their research scholarships (ED481A2021/211, ED481A-2024-083). All authors contributed equally to this work.

References

1 *Alzheimer's Dementia*, 2024, **20**, 3708–3821.
2 F. Chiti and C. M. Dobson, *Annu. Rev. Biochem.*, 2017, **86**, 27–68.
3 E. Fertan, G. Meisl and D. Klenerman, *Alzheimer's Dementia*, 2025, **21**, e70462.
4 K. P. Kepp, N. K. Robakis, P. F. Høilund-Carlsen, S. L. Sensi and B. Vissel, *Brain*, 2023, **146**, 3969–3990.
5 P. H. Nguyen, A. Ramamoorthy, B. R. Sahoo, J. Zheng, P. Faller, J. E. Straub, L. Dominguez, J.-E. Shea, N. V. Dokholyan, A. De Simone, B. Ma, R. Nussinov, S. Najafi, S. T. Ngo, A. Loquet, M. Chiricotto, P. Ganguly, J. McCarty, M. S. Li, C. Hall, Y. Wang, Y. Miller, S. Melchionna, B. Habenstein, S. Timr, J. Chen, B. Hnath, B. Strodel, R. Kayed, S. Lesné, G. Wei, F. Sterpone, A. J. Doig and P. Derreumaux, *Chem. Rev.*, 2021, **121**, 2545–2647.
6 E. N. Cline, M. A. Bicca, K. L. Viola, W. L. Klein, G. Perry, J. Avila, P. I. Moreira, A. A. Sorensen and M. Tabaton, *J. Alzheimer's Dis.*, 2018, **64**, S567–S610.
7 S. J. C. Lee, E. Nam, H. J. Lee, M. G. Savelieff and M. H. Lim, *Chem. Soc. Rev.*, 2017, **46**, 310–323.
8 J. C. Lee, S. J. Kim, S. Hong and Y. S. Kim, *Exp. Mol. Med.*, 2019, **51**, 1–10.
9 K. L. Viola, M. A. Bicca, A. M. Bebenek, D. L. Kranz, V. Nandwana, E. A. Waters, C. R. Haney, M. Lee, A. Gupta, Z. Brahmbhatt, W. Huang, T.-T. Chang, A. Peck, C. Valdez, V. P. Dravid and W. L. Klein, *Front. Neurosci.*, 2022, **15**, DOI: **10.3389/fnins.2021.768646**.
10 M. Novo, S. Freire and W. Al-Soufi, *Sci. Rep.*, 2018, **8**, 1783.
11 S. Illodo, W. Al-Soufi and M. Novo, *Arch. Biochem. Biophys.*, 2024, **761**, 110179.
12 A. A. Reinke, G. A. Abulwerdi and J. E. Gestwicki, *ChemBioChem*, 2010, **11**, 1889–1895.

13 S. Freire, *et al.*, *Dyes Pigm.*, 2014, **110**, 97–105.
14 A. Aliyan, N. P. Cook and A. A. Martí, *Chem. Rev.*, 2019, **119**, 11819–11856.
15 G. Lv, A. Sun, P. Wei, N. Zhang, H. Lan and T. Yi, *Chem. Commun.*, 2016, **52**, 8865–8868.
16 C. Li, L. Yang, Y. Han and X. Wang, *Biosens. Bioelectron.*, 2019, **142**, 111518.
17 Y. Li, D. Xu, A. Sun, S.-L. Ho, C.-Y. Poon, H.-N. Chan, O. T. W. Ng, K. K. L. Yung, H. Yan, H.-W. Li and M. S. Wong, *Chem. Sci.*, 2017, **8**, 8279–8284.
18 C.-H. Chen, Y.-J. Jong, Y.-Y. Chao, C.-C. Wang and Y.-L. Chen, *Anal. Bioanal. Chem.*, 2022, **414**, 8155–8165.
19 J. R. Lakowicz, *Principles of Fluorescence Spectroscopy*, Springer US, Boston, MA, 2006.
20 M. Amaro, D. J. Birch and O. J. Rolinski, *Phys. Chem. Chem. Phys.*, 2011, **13**, 6434–6441.
21 A. g Szabo, K. r Lynn, D. t Krajcarski and D. m Rayner, *FEBS Lett.*, 1978, **94**, 249–252.
22 K. J. Willis and A. G. Szabo, *J. Phys. Chem.*, 1991, **95**, 1585–1589.
23 F. T. S. Chan, G. S. Kaminski Schierle, J. R. Kumita, C. W. Bertoncini, C. M. Dobson and C. F. Kaminski, *Analyst*, 2013, **138**, 2156–2162.
24 D. Pinotsi, L. Grisanti, P. Mahou, R. Gebauer, C. F. Kaminski, A. Hassanali and G. S. Kaminski Schierle, *J. Am. Chem. Soc.*, 2016, **138**, 3046–3057.
25 A. Fricano, F. Librizzi, E. Rao, C. Alfano and V. Vetri, *Biochim. Biophys. Acta, Proteins Proteomics*, 1867, 140258.
26 A. Singh, S. Khatun and A. Nath Gupta, *Chem. Phys. Chem.*, 2020, **21**, 2585–2598.
27 A. Alghamdi, S. Forbes, D. J. S. Birch, V. Vyshemirsky and O. J. Rolinski, *Arch. Biochem. Biophys.*, 2021, **704**, 108886.
28 N. Balasco, C. Diaferia, E. Rosa, A. Monti, M. Ruvo, N. Doti and L. Vitagliano, *IJMS*, 2023, **24**, 8372.